AJNR

MR angiography with ultrashort echo time in cerebral aneurysms treated with Guglielmi detachable coils.

F Gönner, O Heid, L Remonda, G Nicoli, R W Baumgartner, N Godoy and G Schroth

AJNR Am J Neuroradiol 1998, 19 (7) 1324-1328
http://www.ajnr.org/content/19/7/1324

AJNR Am J Neuroradiol 19:1324–1328, August 1998

MR Angiography with Ultrashort Echo Time in Cerebral Aneurysms Treated with Guglielmi Detachable Coils

F. Gönner, O. Heid, L. Remonda, G. Nicoli, R. W. Baumgartner, N. Godoy, and G. Schroth

Summary: We evaluated a time-of-flight three-dimensional MR angiographic sequence with an ultrashort echo time for its ability to characterize the perfusional state of cerebral aneurysms that had been treated with Guglielmi detachable coils and to depict adjacent cerebral arteries. The results were compared with findings at conventional MR angiography and digital subtraction angiography. Adjacent vessels were seen better in 36% of patients imaged with the new technique. Both MR angiographic methods detected residual cerebral aneurysmal perfusion with a tendency to overestimate the patent portion of the aneurysm.

Endovascular electrothrombosis of cerebral aneurysms with electrically detachable platinum coils was established in clinical practice by Guglielmi in 1991 as a viable alternative to surgical clipping in patients in whom the surgical risk is high (1–3). This risk is elevated in patients with severe subarachnoid hemorrhage (Hunt and Hess grade IV and V), those in poor medical condition, or those in whom surgery cannot be performed owing to the anatomic location of the cerebral aneurysm, especially in the posterior circulation.

Whether complete occlusion can be achieved by Guglielmi detachable coils (GDCs) depends on the diameter of the aneurysmal neck (4). Moreover, a recent study in rabbits showed spontaneous reperfusion in 12 of 19 experimental aneurysms of the carotid bifurcation occluded with platinum or tungsten coils, suggesting that GDC treatment may not always be effective in achieving endoluminal thrombosis (5). Therefore, follow up with neuroimaging is mandatory. Cerebral digital subtraction angiography (DSA), however, carries the potential risk of severe complications, such as a cerebrovascular accident. Although this complication is rare, it has drastic consequences for the patient. For this reason, a noninvasive method like MR angiography may be preferred if it can provide excellent characterization of the cerebral vasculature and associated aneurysms (6–8). Recently published preliminary experience with MR angiography of GDC-treated cerebral aneurysms revealed a high sensitivity in identifying the flow within an aneurysm as well as in the adjacent parent and branch vessels. Even better results might be obtained by using shorter echo times (TEs) (9).

Any material whose static magnetic susceptibility differs from that of surrounding tissues will distort the magnetic (B_0) field. In addition, dynamic eddy currents in the conduction of materials caused by time-variable magnetic fields, such as radio frequency (RF) and B_0 gradient fields, may lead to B_1 field homogeneity, image intensity, and distortion artifacts (10). Both effects occur in MR imaging of GDC-treated cerebral aneurysms. The resulting image degradation is the limiting factor in the assessment of the region of interest, especially of adjacent vessels and of the perfusional state of the aneurysmal neck or sac (11). Shortening the TE has been shown to reduce these artifacts significantly (12, 13).

The purpose of this study was to evaluate a new ultrashort-TE three-dimensional (3-D) time-of-flight (TOF) MR angiographic sequence for its ability to reduce GDC-induced susceptibility artifacts so as to increase the detectability of the perfusional state of cerebral aneurysms treated by GDCs and of adjacent cerebral arteries. The results were compared with findings at conventional 3-D TOF MR angiography; DSA was used as the standard of reference.

Methods

Patients

The study group included 14 patients (nine women, five men; 25 to 72 years old; mean age, 50 ± 14 years) with 15 cerebral aneurysms who were examined by DSA, conventional 3-D TOF MR angiography, and ultrashort-TE 3-D TOF MR angiography. Eight patients had aneurysmal subarachnoid hemorrhage with initial Hunt and Hess grades of I or II; six patients had hemorrhage of grades III and IV. In all patients, endovascular treatment was chosen because of elevated surgical risk. After GDC therapy, 15 coiled cerebral aneurysms were

Received May 27, 1997; accepted after revision September 2.
Presented at the annual meeting of the American Society of Neuroradiology, Seattle, June 1996.
From the Departments of Neuroradiology (F.G., O. H., L.R., G.N., G.S.), Neurology (R.W.B.), and Neurosurgery (N.G.), University of Berne, Switzerland.
Address reprint requests to G. Schroth, MD, Department of Neuroradiology, University of Berne, Inselspital, Freiburgstrasse, CH-3010 Bern, Switzerland.

Measurements of GDC-diameters, artifact diameters and perfusional state (DSA, conventional, and ultrashort-TE TOF MR angiography)

Patient	Age, y	Digital Subtraction Angiography		Diameter of Artifacts at MR Angiography (Anteroposterior/Right-Left/Craniocaudal Directions, mm)	
		Extent of Aneurysmal Occlusion	GDC Diameter (Anteroposterior/Right-Left/ Craniocaudal Directions, mm)	Conventional TOF Sequence (TE = 6.0)	Ultrashort TOF Sequence (TE = 2.4)
1	62	Incomplete	6/5/6	12/13/12	10/10/10†
			[3/1/4]*	[3/1/2]*	[6/2/6]*
2	25	Complete	6/5/5	6/6/7	5/5/7†
		Complete	4/4/6	6/7/7	4/4/5
3	61	Complete	5/5/5	12/9/9	10/8/8
4	53	Complete	4/3/3	7/7/8	6/6/7
5	57	Incomplete	15/14/10	20/19/13	18/18/12
			[8/6/10]*	[9/9/13]*	[9/9/15]*
6	49	Complete	9/6/5	13/11/9	8/10/8
7	35	Complete	4/4/6	11/8/11	8/7/8
		Complete	4/4/6	10/8/12	7/7/8
8	36	Complete	5/6/5	10/12/9	8/9/6
9	41	Incomplete	7/9/12	12/10/17	8/8/14†
			[4/10/12]*	[9/12/10]*	[8/12/12]*
10	56	Incomplete	10/9/10	15/13/10	13/10/10
			[4/4/10]*	[8/8/10]*	[8/8/10]*
11	59	Incomplete	16/12/14	20/19/17	19/18/15
			[9/8/16]*	[10/10/14]*	[10/10/14]*
12	72	Complete	5/5/5	8/9/8	7/6/3
13	34	Complete	5/8/5	13/18/10	9/9/5†
14	67	Complete	4/2/5	12/10/10	8/8/8†
		Complete	4/2/4	12/10/10	9/8/8†
		Complete	5/2/5	12/10/10	8/7/8†

* Maximum extent of perfused area in brackets.

† Improved depiction of adjacent vessels.

assessed. One patient underwent MR angiography on the same day of treatment and at 54 days after treatment. Another patient was examined on the same day of treatment, at 25 weeks, and again at 45 weeks after initial DSA. Otherwise, the time interval between DSA and MR angiography was less than 1 week in 14 patients, 1½ weeks in one patient, and 6 weeks in two patients. One patient had two aneurysms, one each of the right and left posterior inferior cerebellar artery (PICA). In all, the data of 18 comparative measurements were included (see Table).

Ultrashort-TE and Conventional 3-D TOF MR Angiography

A 3-D TOF fast low-angle shot (FLASH) MR angiographic sequence with an ultrashort TR of 6.3, an ultrashort TE of 2.4, two excitations, and an 8° flip angle gaussian RF pulse (6.3/2.4/2/8) was implemented on a 1.5-T MR scanner (Fig 1A). One hundred and twenty-eight axial images were generated. The imaging parameters included a section thickness of 1.0 mm, a resolution matrix of 192 × 256, a field of view of 200 × 150

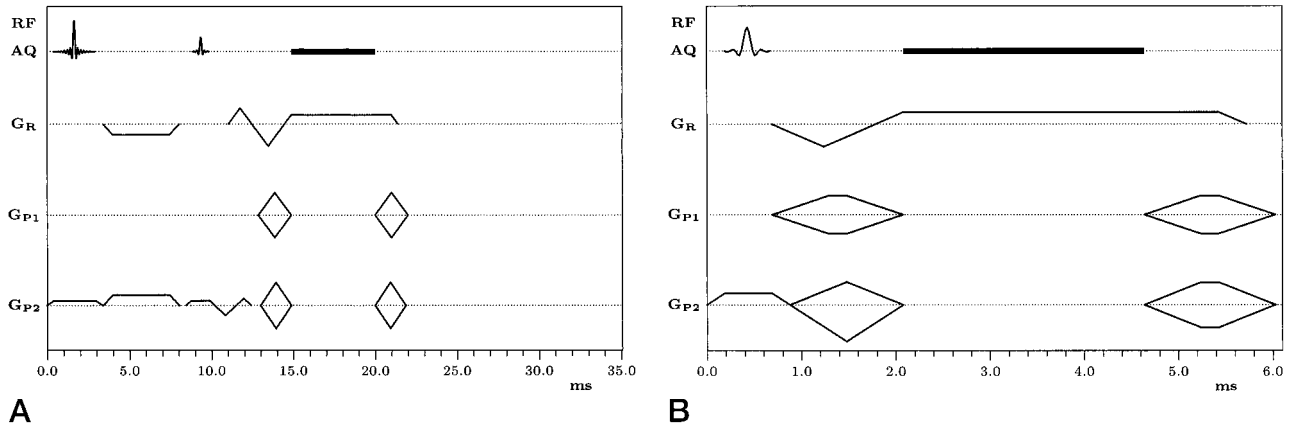

FIG 1. The ultrashort-TE and conventional 3-D TOF MR angiographic sequences. RF, radio frequency; AQ, acquisition; G_R, readout gradient; G_{P1}, 2-D phase-encoding gradient; G_{P2}, 3-D phase-encoding gradient; ms, milliseconds.

A, Ultrashort-TE 3-D TOF MR angiographic sequence (6.3/2.4/2/8): 3-D RF-spoiled fast low-angle shot (FLASH) sequence.

B, Conventional 3-D TOF (FLASH) MR angiographic sequence (35/6.0/1/20) with regional saturation pulse and gradient motion refocusing in readout section directions.

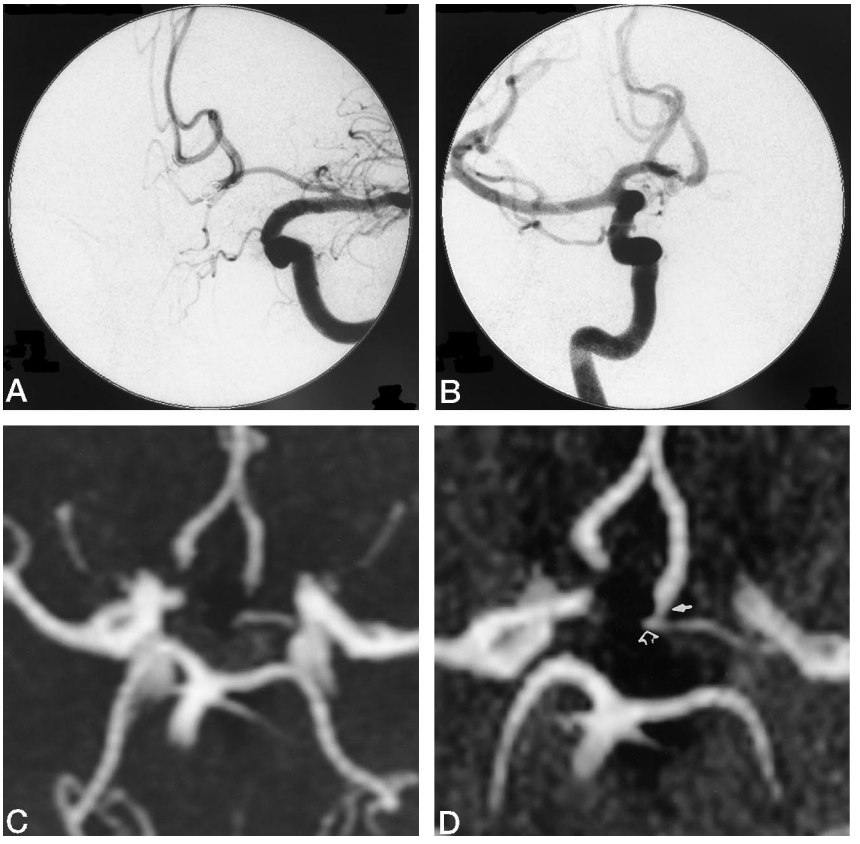

FIG 2. Case 14: A 67-year-old man with subarachnoid hemorrhage Hunt and Hess grade I. DSA revealed a 4 × 4 × 6-mm ACoA aneurysm pointing in the dorsocaudal direction. The left anterior cerebral artery (ACA) was hypoplastic and the aneurysm was fed mainly by the right ACA. Complete occlusion of the aneurysm was proved on both immediate postinterventional DSA/MR angiography and repeated control-DSA/MR angiography 25 and 43 weeks later.

A, Postinterventional left carotid DSA in left oblique Towne projection shows the GDC completely occluding the ACoA aneurysm. The left ACA is hypoplastic in the A1 segment. The A2 segment is patent.

B, Postinterventional right carotid DSA, Towne projection, shows the mainly feeding right A1 segment of the ACA, the completely occluded aneurysm, and both patent A2 segments.

C, Conventional MR angiography (35/6.0/1/20), MIP image, fails to show the distal part of the right A1 segment, the ACoA, and both proximal A2 segments.

D, Ultrashort-TE MR angiography (6.3/2.4/2/8), MIP image, shows the distal part of the right A1 and a part of the left ACoA origin (*open arrow*). The course of the A1 to A2 segment is shown (*solid arrow*).

mm, two acquisitions, and a total acquisition time of 309 seconds. The parameters for the conventional MR angiographic sequence supplied by the manufacturer (35/6.0/1/20) included a section thickness of 1.0 mm, a resolution matrix of 165 × 256, a field of view of 200 × 150 mm, one acquisition, and a total acquisition time of 233 seconds (Fig 1B).

The extent of the GDC-induced signal loss due to the susceptibility artifacts in the region of interest was quantified by measuring the maximum diameters in the anteroposterior, right-left, and craniocaudal directions on the filmed images. The craniocaudal diameter was calculated by subtracting the section positions of the most cranial and caudal sections showing recognizable artifacts. To reduce observer errors, the measurements were done by two experienced neuroradiologists who were blinded to the results of DSA. Occlusion was defined as the absence of a flow signal in the region of the assumed aneurysm inside the volume of the susceptibility artifact. If any flow signal inside the region circumscribed by the susceptibility artifact was seen, aneurysmal occlusion was considered to be incomplete. In this case, the extent of the perfused area was measured in anteroposterior, right-left, and craniocaudal directions as well as on the DSA images (see below).

Digital Subtraction Angiography

Selective intraarterial X-ray DSA was performed on a dedicated neurointerventional biplane system, consisting of two imaging devices arranged on a G-ring at a mechanically stable, fixed 90° angle. A CCD digital camera with a 1024 × 1024 matrix resulted in a spatial resolution of 0.16 to 0.32 mm, depending on the magnification factor of the image intensifier. The system's integrated software allows diameter measurements of the vessels and the GDCs in the isocenter of the DSA image. The accuracy of this system was studied with phantoms, and the measurement error was found to be less than 0.05 mm on average and 0.50 mm at maximum (14). During postprocessing, the maximum diameter of the coil mesh outline was calculated in anteroposterior, right-left, and craniocaudal directions by the DSA examiner. Incomplete occlusion was defined as partial filling of the aneurysm with contrast medium. Occlusion was complete when no contrast medium was present either in the neck or the sac of the aneurysm. If any contrast medium was seen in the neck or the sac, the extent of the perfused area was measured in the same anteroposterior, right-left, and craniocaudal directions.

Extent of GDC-Induced Signal Dropout

The artificial overestimation factor of the coil mesh on MR angiograms was calculated according to the formula α = d(MR angiography)/d(angio), with d(MR angiography) being the maximum diameter of coil-induced artifacts on the MR angiograms and d(angio) the maximum diameter of the coils on biplane DSA images. To estimate the difference in artificial overestimation for both MR angiographic sequences, α was calculated independently for each plane and each direction. Statistical analysis was performed in all 54 directions using the nonparametric Mann-Whitney *U*-test.

Results

The maximum diameters of the areas of signal loss in the anteroposterior, right-left, and craniocaudal directions of the 18 measurements are given in the Table. The overestimation factor, α, for the conventional MR angiograms was 2.03 ± 0.88 (mean ± 1 SD) and was significantly different (P .0002, Mann-Whitney *U*-test) from α = 1.57 ± 0.68 at ultrashort-TE MR angiography.

In five (33%) of 15 aneurysms, the occlusion was angiographically incomplete (cases 1, 6, 10, 11, 12). Both conventional and ultrashort-TE MR angiogra-

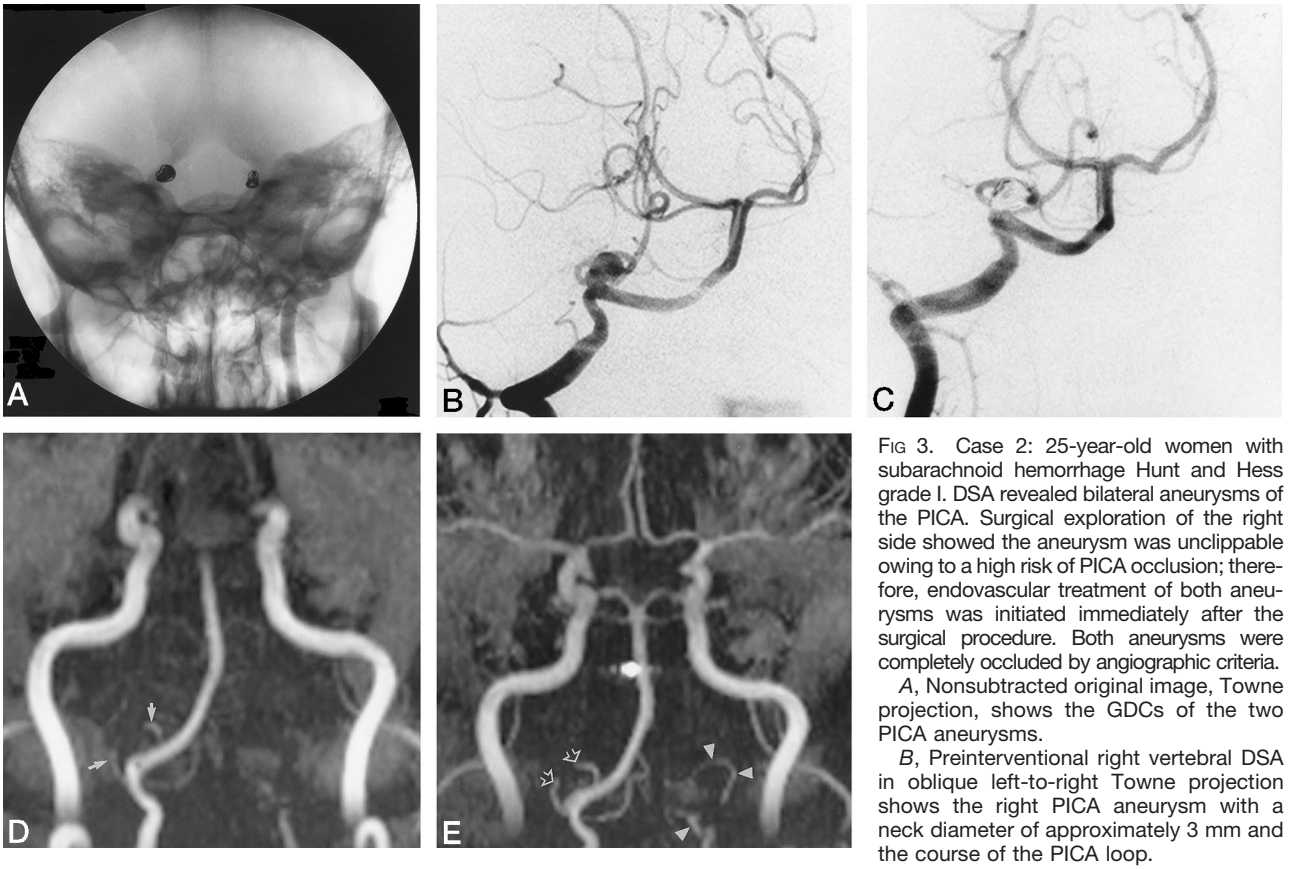

FIG 3. Case 2: 25-year-old women with subarachnoid hemorrhage Hunt and Hess grade I. DSA revealed bilateral aneurysms of the PICA. Surgical exploration of the right side showed the aneurysm was unclippable owing to a high risk of PICA occlusion; therefore, endovascular treatment of both aneurysms was initiated immediately after the surgical procedure. Both aneurysms were completely occluded by angiographic criteria.

A, Nonsubtracted original image, Towne projection, shows the GDCs of the two PICA aneurysms.

B, Preinterventional right vertebral DSA in oblique left-to-right Towne projection shows the right PICA aneurysm with a neck diameter of approximately 3 mm and the course of the PICA loop.

C, Postinterventional right vertebral digital subtraction angiogram, Towne projection, shows the marked loop of the right PICA, partially hidden by the GDC.

D, Conventional MR angiography (35/6.0/1/20), MIP image, shows complete occlusion of the PICA aneurysm. Parts of the adjacent right PICA loop are missed and less intense (*arrows*). The left PICA is not seen.

E, Ultrashort-TE MR angiography (6.3/2.4/2/8), MIP image, shows more flow signal in the adjacent right PICA loop (*open arrows*) with more intense contrast as comparison with conventional MR angiography. Note the left PICA loop (*arrowheads*), which was not seen on conventional MR angiograms.

phy gave identical results on axial images, as did DSA. There was a slight increase in diameter of the perfused area on the MR angiograms compared with that on the DSA images (see Table). In one case, the extent of perfusion was relatively small. This was detected by conventional MR angiography on the axial images, but a vessel dropout was observed on maximum intensity projection (MIP) images. Ultrashort-TE MR angiography showed the perfusional state both on the axial and MIP images.

In five (36%) of 14 patients, adjacent vessels were shown better by the ultrashort-TE MR angiographic technique. This advantage over conventional MR angiography is due to reduction of susceptibility artifacts, as illustrated in Figures 2 and 3. Improved visibility of a flow signal in adjacent vessels (parts of the anterior communicating artery [ACoA] and A1 segments) was evident in three patients with GDC-treated cerebral aneurysms of the ACoA (Fig 2). Flow in both posterior cerebral arteries (P1 segments) was detected in a GDC-treated basilar tip aneurysm in one patient; in another patient, more parts of the PICA loop surrounding a GDC-treated cerebral aneurysm could be seen with the new technique (Fig 3).

Discussion

In a study of 43 MR angiograms obtained in 23 patients as follow-up of GDC-treated cerebral aneurysms, Derdeyn and coworkers (9) detected the patency of parent arteries with a sensitivity of 96%. Residual aneurysmal flow was identified with a lower sensitivity (71%) and specificity (89%). The authors concluded that this technique may be a useful adjunct to DSA in some clinical situations. They pointed out that the flow in smaller vessels may sometimes be obscured and that better results might be obtained by using shorter TEs than 5.3 to 5.7.

The basic idea of the new sequence applied in the present work is the absence of gradient motion refocusing in favor of a shorter TE and TR (Sayre J, Wright A. Short gradient imaging of the heart. Presented at the annual meeting of the Society of Magnetic Resonance in Medicine, 1988). Besides a reduced higher-order motion sensitivity, the TE reduction, as compared with the conventional 3-D TOF MR angiographic sequence supplied by the manufacturer, and the higher readout bandwidth (390 Hz per pixel versus 195 Hz per pixel) aim mainly to reduce static B_0 inhomogeneity artifacts induced by

metal implants. The short TR enables coverage of the entire head volume, eliminating the need for the commonly used venous selective RF saturation. The result is an improved signal-to-noise (SNR) ratio, comparable to the conventional MR angiographic sequence despite the higher readout bandwith, which alone would result in a drop in SNR to $\sqrt{}$(195 Hz/390 Hz) = 70.7%. Furthermore, absence of the RF saturation pulse decreases the specific absorption rate and minimizes problems with spoiling of unwanted signals.

The results of the 18 comparative measurements performed in our study showed that the ultrashort-TE MR angiographic technique can depict more parts of diagnostically relevant adjacent vessels by reducing the extent of coil-induced artifacts. For both conventional and ultrashort-TE MR angiography, the detection of residual aneurysmal perfusion was identical to that provided by DSA. Furthermore, there was a slight increase in diameter of the perfused area on the MR angiograms as compared with DSA images. This may indicate that MR angiography overestimates the patent portion of the GDC-treated cerebral aneurysm and could depict small residual necks with a high sensitivity, an indicator of a useful screening method. Although these data suggest a higher sensitivity than reported in the study by Derdeyn et al (9), the paucity of patients limits a reliable determination of the sensitivity and specificity of each method. Another limitation is that we did not determine the impact of the new ultrashort-TE MR angiographic sequence on therapy and outcome. However, we think that the improved detectability of adjacent vessels and the possibly higher sensitivity in detecting residual aneurysmal flow could lead to a more restrictive use of DSA in the follow-up of GDC-treated cerebral aneurysms. A third limitation is that we did not use threshold criteria to determine the extent of the susceptibility artifacts, which might be the reason for the relatively high standard deviation of the overestimation factor, α. As a consequence, the size of the artifacts is not a reliable indicator of the size of the coil collection in our study. Therefore, X-ray DSA remains the diagnostic method of choice for the assessment of GDC integrity.

Conclusion

The ultrashort-TE 3-D TOF sequence improves the ability of MR angiography in the follow-up of GDC-treated cerebral aneurysms for the assessment of adjacent vessels by reducing GDC-induced signal dropout. For detectability of residual aneurysmal flow, the reduction in TE has no advantage over conventional MR angiographic sequences. Both MR angiographic sequences tended to overestimate residual cerebral aneurysmal perfusion. The sensitivity of the latter and the clinical impact of the ultrashort-TE sequence, especially as a screening examination for patency of cerebral aneurysms, must be determined in further studies.

References

1. Guglielmi G, Vinuela F, Sepetka I, Macellari V. **Electrothrombosis of saccular aneurysms via endovascular approach, 1: electrochemical basis, technique, and experimental results.** *J Neurosurg* 1991; 75:1–7
2. Guglielmi G, Vinuela F, Dion J, Duckwiler G. **Electrothrombosis of saccular aneurysms via endovascular approach, 2: preliminary clinical experience.** *J Neurosurg* 1991;75:8–14
3. Guglielmi G, Vinuela F, Duckwiler G, et al. **Endovascular treatment of posterior circulation aneurysms by electrothrombosis using electrically detachable coils.** *J Neurosurg* 1992;77:515–524
4. Zubillaga AF, Guglielmi G, Vinuela F, Duckwiler G. **Endovascular occlusion of intracranial aneurysms with electrically detachable coils: correlation of aneurysm neck size and treatment results.** *AJNR Am J Neuroradiol* 1994;15:815–820
5. Reul J, Weis J, Spetzger U, et al. **Long-term angiographic and histopathologic findings in experimental aneurysms of the carotid bifurcation embolized with platinum and tungsten coils.** *AJNR Am J Neuroradiol* 1997;18:35–42
6. Sevick RS, Tsurada JS, Schmalbrock P. **Three-dimensional TOF MR angiography in the evaluation of cerebral aneurysms.** *J Comput Assist Tomogr* 1990;14:874–881
7. Bontozoglou N, Spanos H, Lasjaunias P, Zarifis G. **Three-dimensional display of the orifice of intracranial aneurysms: a new potential application for magnetic resonance angiography.** *Neuroradiology* 1994;36:346–349
8. Horikoshi T, Fukamachi, Nishi H, Fukasawa I. **Detection of intracranial aneurysms by three-dimensional TOF magnetic resonance angiography.** *Neuroradiology* 1994;36:203–207
9. Derdeyn CP, Graves VB, Turski PA, Masaryk AM, Strother CM. **MR angiography of saccular aneurysms after treatment with Guglielmi detachable coils: preliminary experience.** *AJNR Am J Neuroradiol* 1997;18:279–286
10. Camacho CR, Plewes DB, Henkelman RM. **Nonsusceptibility artifacts due to metallic objects in MR imaging.** *J Magn Reson Imaging* 1995;5:75–88
11. Wilcock DJ, Jaspan T, Worthington BS. **Problems and pitfalls of 3-D TOF magnetic resonance angiography of the intracranial circulation.** *Clin Radiol* 1995;50:526–532
12. Schmalbrock P, Yuan C, Chakeres DW, Kohli J, Pelc NJ. **Volume MR angiography: methods to achieve very short echo times.** *Radiology* 1990;175:861–865
13. Wehrli FW, Chao PW, Youssem DM. **Parameter dependence of susceptibility-induced signal losses in gradient-echo imaging.** *Magn Reson Imaging* 1989;7:139
14. Toennies KD, Oishi S, Koster D, Schroth G. **Accuracy of distance measurements in biplane angiography. In: Kim Y, ed.** *Proceedings of SPIE: The International Society for Optical Engineering.* Bellingham, WA: 1997;3031:19–30